J|A|C|S ARTICLES

Published on Web 11/15/2010

Computational Study of Silica-Supported Transition Metal Fragments for Kubas-type Hydrogen Storage

Claire V. J. Skipper,[†] Ahmad Hamaed,[‡] David M. Antonelli,*[,§] and Nikolas Kaltsoyannis*[,†]

Department of Chemistry, University College London, 20 Gordon Street, London WC1H OAJ, United Kingdom, Department of Chemistry and Biochemistry, University of Windsor, 401 Sunset Avenue, Windsor, Ontario N9B 3P4, Canada, and Sustainable Environment Research Centre, University of Glamorgan, Pontypridd CF37 1DL, United Kingdom

Received August 20, 2010; E-mail: n.kaltsoyannis@ucl.ac.uk

Abstract: To verify the role of the Kubas interaction in transition metal grafted mesoporous silicas, and to rationalize unusual rising enthalpy trends with surface coverage by hydrogen in these systems, computational studies have been performed. Thus, the interaction of H_2 with the titanium centers in molecular models for experimentally characterized mesoporous silica-based H_2 absorption materials has been studied quantum chemically using gradient corrected density functional theory. The interaction between the titanium and the H_2 molecules is found to be of a synergic, Kubas type, and a maximum of four H_2 molecules can be bound to each titanium, in good agreement with previous experiments. The average Ti−H_2 interaction energies in molecules incorporating benzyl ancillary ligands (models of the experimental systems) increase as the number of bound H_2 units increases from two to four, in agreement with the experimental observation that the H_2 adsorption enthalpy increases as the number of adsorbed H_2 molecules increases. The Ti−H_2 interaction is shown to be greater when the titanium is bound to ancillary ligands, which are poor π-acceptors, and when the ancillary ligand causes the least steric hindrance to the metal. Extension of the target systems to vanadium and chromium shows that, for molecules containing hydride ancillary ligands, a good relationship is found between the energies of the frontier molecular orbitals of the molecular fragments, which interact with incoming H_2 molecules, and the strength of the M−H_2 interaction. For the benzyl systems, both the differences in M−H_2 interaction energies and the energy differences in frontier orbital energies are smaller than those in the hydrides, such that conclusions based on frontier orbital energies are less robust than for the hydride systems. Because of the high enthalpies predicted for organometallic fragments containing hydride ligands, and the low affinity of Cr(III) for hydrogen in this study, these features may not be ideal for a practical hydrogen storage system.

1. Introduction

To replace our dependence on depleting fossil fuels and reduce greenhouse gas emissions, alternative energy sources and carriers are sought. Hydrogen is under consideration as a clean energy carrier due to its high energy density (142 MJ kg^{-1}) when compared to liquid hydrocarbons (47 MJ kg^{-1})[1] and because when burnt cleanly water is the only byproduct.[1,2]

45 m^3 of hydrogen at room temperature and pressure is required for a hydrogen fuel cell powered car to travel 400 km,[1] and it is the onboard storage of this hydrogen that still remains a problem. Methods for its containment include storing it as a high pressure gas, as a liquid, or adsorbing it onto a support or solid. The U.S. Department of Energy has targets to be met by 2015 for these storage systems, which include a gravimetric storage density of 0.055 kgH_2 kg^{-1}, a volumetric storage capacity of 0.040 kgH_2/L, and a 3 min refueling time.[3] These targets are even more stringent for the hydrogen adsorption materials as they apply to the whole system and not just the material. It has been calculated that to achieve these storage requirements the adsorption enthalpy of the material should be between 20 and 40 kJ mol^{-1}.[4,5]

At present, the two main types of storage material adsorb hydrogen either by physisorption, with adsorption enthalpies of ca. 3−6 kJ mol^{-1},[6] or by chemisorption with typical hydrogen adsorption enthalpies of 40−80 kJ mol^{-1}.[7,8] Materials that physisorb the hydrogen bind weakly to the hydrogen with hardly

[†] University College London.
[‡] University of Windsor.
[§] University of Glamorgan.

(1) Schlapbach, L.; Zuttel, A. *Nature* **2001**, *414*, 353.
(2) Balat, M. *Int. J. Hydrogen Energy* **2008**, *33*, 4013.
(3) Hydrogen, Fuel Cells and Infrastructure Technologies Program: Multi-Year Research, Development and Demonstration Plan: Planned Program Activities for 2005−2015. Section 3.3 Hydrogen Storage, 2007; http://www1.eere.energy.gov/hydrogenandfuelcells/mypp/pdfs/storage.pdf (accessed March 16, 2010).
(4) Lochan, R. C.; Head-Gordon, M. *Phys. Chem. Chem. Phys.* **2006**, *8*, 1357.
(5) Rowsell, J. L. C.; Yaghi, O. M. *Angew. Chem., Int. Edit.* **2005**, *44*, 4670.
(6) van den Berg, A. W. C.; Arean, C. O. *Chem. Commun.* **2008**, 668.
(7) Hoang, T. K. A.; Antonelli, D. M. *Adv. Mater.* **2009**, *21*, 1787.
(8) Orimo, S. I.; Nakamori, Y.; Eliseo, J. R.; Zuttel, A.; Jensen, C. M. *Chem. Rev.* **2007**, *107*, 4111.

 10.1021/ja107539j

any change in the H−H bond length. They are usually porous with large surface areas to maximize the adsorption capacity and include zeolites, carbon-based materials, and polymers.[6] Materials that adsorb the hydrogen by chemisorption break the H−H bond and form strong chemical bonds with the hydrogen atoms. These materials include metal and complex hydrides. To achieve an adsorption enthalpy in the desired range, between these two extremes, metal sites have been engineered into a variety of physisorption materials. The hydrogen molecules interact with these metals in a Kubas fashion,[9,10] which raises the average hydrogen adsorption enthalpy of the material.

A Kubas interaction[9,10] is consistent with a lengthening of the H−H bond without breakage and involves a σ-donation from the H_2 molecule's σ-bonding orbital into an empty d orbital of a metal and a π-back-donation from the metal's filled d orbital into the σ^* antibonding orbital of the H_2 molecule. This is similar to the synergic bonding described by the Dewar−Chatt−Duncanson model for the interaction of, for example, CO with transition metals.[11,12]

Systems where metals have been included to promote Kubas interaction have been studied both computationally and experimentally and include boron-doped graphene sheets,[13−15] nanotubes,[16,17] and fullerenes decorated with metal atoms,[18−20] ethylene with a titanium atom bound to it,[21−23] metal organic frameworks with open metal sites,[24−26] polymers decorated with metals,[27] metals bound to the functional groups of hydrocarbons,[22,28,29] and boranes substituted with metals.[30] It has been found that the hydrogen may bind to the metal initially as a hydride[21,23,29] or molecularly.[27,30] When the hydrogen binds to a transition metal in a molecular fashion, it tends to do so with a lengthening of the H−H bond, and the bonding mode can be explained using a Kubas model.[22,27−30] This is not always the case for other metals.[18,31]

We have recently presented materials in which the H_2 is thought to bind to the metals via a Kubas interaction.[7,32−34] These systems consist of 5−10 wt % of organometallic Ti, V, and Cr fragments grafted onto mesoporous silica and are of great interest because of the unusual behavior of the enthalpies, which rise on surface coverage, suggesting that physisorption in these systems is accompanied by a second mechanism likely involving weak chemisorption. The isotherms of these materials are also unusual in that they do not saturate at 77 K and 80 bar and possess large linear regions. This behavior is also observed in new metal hydrazide systems developed by our group.[34] These materials have higher activities than the silica-supported systems and greatly reduce the physisorption component by minimizing surface area and increasing the concentration of unsaturated metal sites in the material. While the rising enthalpies must be considered an approximation based on the Clausius−Claperyon equation, and the enthalpies are an average of contributions from physisorption and weak chemisorption, this trend must be considered valid because subtracting out the contribution from physisorption from a pristine silica surface (which decreases from 5 to 3 kJ mol^{-1} on surface coverage) yields a function with enthalpies that increase even more steeply on surface coverage.

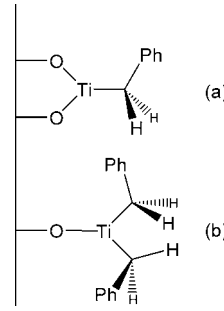

Figure 1. Schematic representations of (a) a benzyl disiloxy Ti(III) binding site and (b) a dibenzyl siloxy Ti(III) binding site.

In the present work, we seek to model the silica-supported titanium system computationally. The target system has been characterized experimentally as a mesoporous silica with 23 Å wide pores and titanium binding sites over the entire surface.[33] There are two types of H_2 binding site in the solid. In one type, the titanium binds to the silica surface through two Ti−O bonds with one ancillary benzyl ligand, while in the other, the titanium is attached to the silica surface with one Ti−O bond and has two ancillary benzyl ligands. These are distributed in a 55:45 ratio in favor of binding site (a) (Figure 1). The number of H_2 molecules adsorbed and the H_2 adsorption enthalpy increase with increasing pressure up to maxima of 2.7 H_2 units per Ti and 22.14 kJ mol^{-1}, respectively, at 77 K and 80 bar. When the material's properties were optimized, these maxima rose to 3.98 H_2 per Ti and 23 kJ mol^{-1}, respectively,[32] and further exploration showed that, prior to decomposition of the material, the number of H_2 molecules accommodated rose to 4.85 H_2 per Ti center.[35] These results are of special interest because a maximum of two Kubas H_2 ligands have been observed in isolable organometallic systems,[36] and the enthalpy is clearly within the desired range for optimum H_2 storage. Subsequent investigations altered the ancillary ligand from benzyl to methyl or allyl,[32] although in the latter systems THF remained bound to the Ti,

(9) Kubas, G. J. *J. Organomet. Chem.* **2001**, *635*, 37.
(10) Kubas, G. J. *J. Organomet. Chem.* **2009**, *694*, 2648.
(11) Dewar, J. S. *Bull. Soc. Chim. Fr.* **1951**, *18*, C71.
(12) Chatt, J.; Duncanson, L. A. *J. Chem. Soc.* **1953**, 2939.
(13) Rojas, M. I.; Leiva, E. P. M. *Phys. Rev. B* **2007**, *76*, 155415.
(14) Kim, G.; Jhi, S. H. *J. Phys. Chem. C* **2009**, *113*, 20499.
(15) Kim, G.; Jhi, S. H.; Lim, S.; Park, N. *Phys. Rev. B* **2009**, *79*, 155437.
(16) Yildirim, T.; Ciraci, S. *Phys. Rev. Lett.* **2005**, *94*, 175501.
(17) Shevlin, S. A.; Guo, Z. X. *J. Phys. Chem. C* **2008**, *112*, 17456.
(18) Wu, G. F.; Wang, J. L.; Zhang, X. Y.; Zhu, L. Y. *J. Phys. Chem. C* **2009**, *113*, 7052.
(19) Zhao, Y. F.; Kim, Y. H.; Dillon, A. C.; Heben, M. J.; Zhang, S. B. *Phys. Rev. Lett.* **2005**, *94*, 155504.
(20) Sun, Q.; Wang, Q.; Jena, P.; Kawazoe, Y. *J. Am. Chem. Soc.* **2005**, *127*, 14582.
(21) Durgun, E.; Ciraci, S.; Zhou, W.; Yildirim, T. *Phys. Rev. Lett.* **2006**, *97*, 226102.
(22) Zhou, W.; Yildirim, T.; Durgun, E.; Ciraci, S. *Phys. Rev. B* **2007**, *76*, 085434.
(23) He, N.; Gao, T.; Zhang, Z. H.; Tian, X. F.; Han, H. L. *J. Mol. Struct. (THEOCHEM)* **2009**, *916*, 147.
(24) Kaye, S. S.; Long, J. R. *J. Am. Chem. Soc.* **2008**, *130*, 806.
(25) Lochan, R. C.; Khaliullin, R. Z.; Head-Gordon, M. *Inorg. Chem.* **2008**, *47*, 4032.
(26) Dinca, M.; Dailly, A.; Liu, Y.; Brown, C. M.; Neumann, D. A.; Long, J. R. *J. Am. Chem. Soc.* **2006**, *128*, 16876.
(27) Lee, H.; Choi, W. I.; Ihm, J. *Phys. Rev. Lett.* **2006**, *97*, 056104.
(28) Lee, H.; Nguyen, M. C.; Ihm, J. *Solid State Commun.* **2008**, *146*, 431.
(29) Nguyen, M. C.; Lee, H.; Ihm, J. *Solid State Commun.* **2008**, *147*, 419.
(30) Zhang, C. G.; Zhang, R. W.; Wang, Z. X.; Zhou, Z.; Zhang, S. B.; Chen, Z. F. *Chem.-Eur. J.* **2009**, *15*, 5910.
(31) Zhou, W.; Yildirim, T. *J. Phys. Chem. C* **2008**, *112*, 8132.
(32) Hamaed, A.; Hoang, T. K. A.; Trudeau, M.; Antonelli, D. M. *J. Organomet. Chem.* **2009**, *694*, 2793.
(33) Hamaed, A.; Trudeau, M.; Antonelli, D. M. *J. Am. Chem. Soc.* **2008**, *130*, 6992.
(34) Mai, H. V.; Hoang, T. K. A.; Hamaed, A.; Trudeau, M.; Antonelli, D. M. *Chem. Commun.* **2010**, *46*, 3206.
(35) Hamaed, A.; Van Mai, H.; Hoang, T. K. A.; Trudeau, M.; Antonelli, D. *J. Phys. Chem. C* **2010**, *114*, 8651.
(36) Kubas, G. J. *Chem. Rev.* **2007**, *107*, 4152.

precluding direct comparisons with the benzyl material. Other studies compared the role of metal and oxidation state and found that, in general, the H_2 storage ability of materials decreases in the order Ti > V > Cr and $M^{2+} > M^{3+}$.[35] Some of these systems also showed an improvement on hydrogenation that was consistent with a reduction of the metal center and/or replacement of an alkyl ligand on the metal with a hydride by σ bond metathesis.

In this computational investigation, we model quantum chemically, using gradient-corrected density functional theory (DFT), the Ti binding sites in the experimentally characterized systems, and their interactions with H_2. Following literature precedent,[21,22,25,37−39] we have chosen to model the binding sites as molecules. The Kubas model is, as discussed above, characterized in terms of molecular orbital interactions, and hence a computational approach based on molecular orbital theory is a logical tool for the present study. We verify the role of the Kubas interaction (only postulated thus far because of the difficulty in performing spectroscopy on the silica-supported systems) and reproduce and explain the counterintuitive experimental result of increasing H_2 adsorption enthalpy with the number of H_2 molecules bound. We also alter the model of the experimental system to observe the effect on the hydrogen adsorption. Specifically, the ancillary ligand is altered from benzyl to allyl, methyl, or hydride and the metal from Ti to V or Cr.

2. Computational Details

The titanium binding sites of the mesoporous silica[33] were modeled as molecules with the bulk silica truncated with hydrogen atoms (Figure 2A and E). The binding sites with no H_2 units bound were first geometry optimized, and then the positions of the atoms in the part of the molecule representing the silica surface were fixed, to represent the inflexibility of the bulk silica. The fixed atoms were those from the silicon atoms onward moving away from the titanium. H_2 units were then bound to the titanium, and the unfixed portion of the molecule was allowed to optimize.

Spin-unrestricted DFT, with the Perdew−Burke−Ernzerhof (PBE)[40,41] exchange correlation functional, was used throughout. This functional was chosen after test calculations with a range of functionals (VWN,[42] BLYP,[43−46] PBE with dispersion,[47] and B3LYP[48]) showed that the trends in the Ti−H_2 interaction energies were very similar, regardless of functional. PBE was selected as it gave absolute Ti−H_2 interaction energies that were closest to the experimentally determined hydrogen adsorption enthalpies (Supporting Information Figure 1).

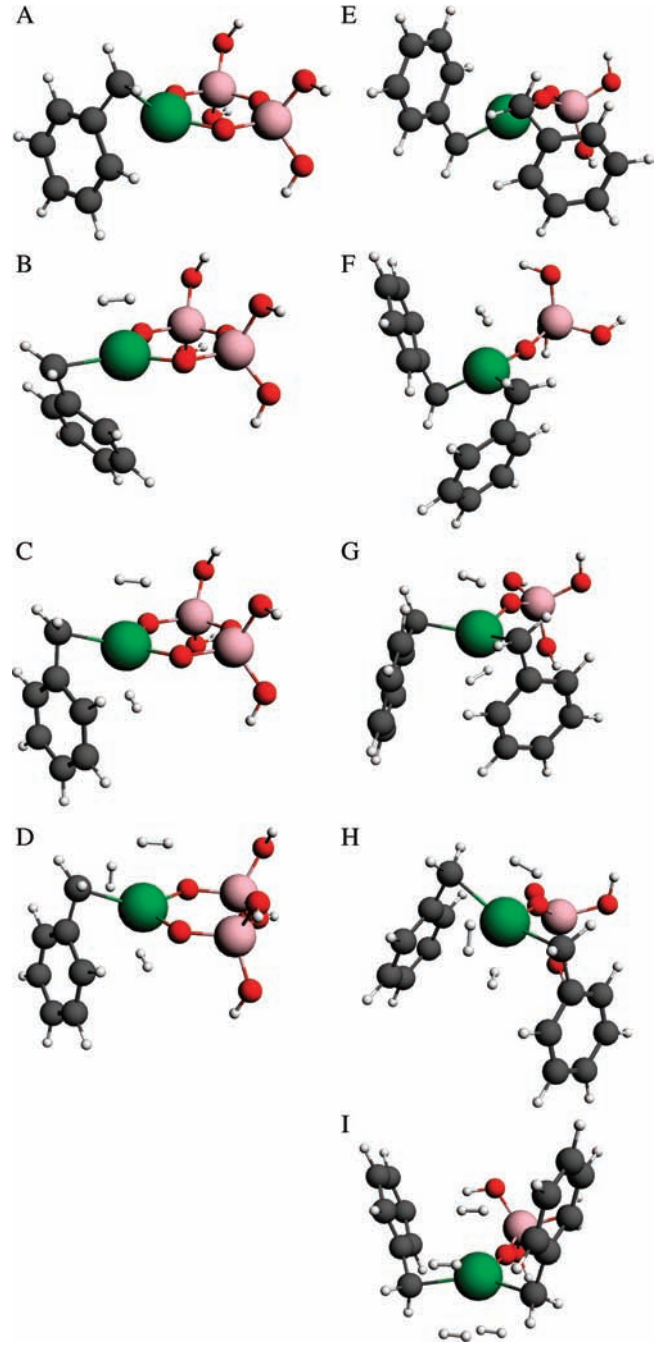

Figure 2. Ball-and-stick representations of the optimized geometries of the molecules representing the binding sites. Binding site representation (a) with (A) zero, (B) one, (C) two, and (D) three H_2 molecules bound. Binding site representation (b) with (E) zero, (F) one, (G) two, (H) three, and (I) four H_2 molecules bound. Key: C black, H white, O red, Si peach, Ti green.

The Gaussian 03 code[49] was used for all geometry optimizations, and the 6-311++G** basis[50−56] sets were used on all atoms. An ultrafine integration grid was used, and the rms force geometry

(37) Kosa, M.; Krack, M.; Cheetham, A. K.; Parrinello, M. *J. Phys. Chem. C* **2008**, *112*, 16171.
(38) Mavrandonakis, A.; Klontzas, E.; Tylianakis, E.; Froudakis, G. E. *J. Am. Chem. Soc.* **2009**, *131*, 13410.
(39) Wong, M.; Van Kuiken, B. E.; Buda, C.; Dunietz, B. D. *J. Phys. Chem. C* **2009**, *113*, 12571.
(40) Perdew, J. P.; Burke, K.; Ernzerhof, M. *Phys. Rev. Lett.* **1996**, *77*, 3865.
(41) Perdew, J. P.; Burke, K.; Ernzerhof, M. *Phys. Rev. Lett.* **1997**, *78*, 1396.
(42) Vosko, S. H.; Wilk, L.; Nusair, M. *Can. J. Phys.* **1980**, *58*, 1200.
(43) Becke, A. D. *Phys. Rev. A* **1988**, *38*, 3098.
(44) Lee, C. T.; Yang, W. T.; Parr, R. G. *Phys. Rev. B* **1988**, *37*, 785.
(45) Johnson, B. G.; Gill, P. M. W.; Pople, J. A. *J. Chem. Phys.* **1993**, *98*, 5612.
(46) Russo, T. V.; Martin, R. L.; Hay, P. J. *J. Chem. Phys.* **1994**, *101*, 7729.
(47) Grimme, S. *J. Comput. Chem.* **2006**, *27*, 1787.
(48) Stephens, P. J.; Devlin, F. J.; Chabalowski, C. F.; Frisch, M. J. *J. Phys. Chem.* **1994**, *98*, 11623.
(49) Frisch, M. J.; et al. *Gaussian 03*, revision E.01; Gaussian, Inc.: Wallingford, CT, 2004. (See the Supporting Information for full reference.)
(50) McLean, A. D.; Chandler, G. S. *J. Chem. Phys.* **1980**, *72*, 5639.
(51) Krishnan, R.; Binkley, J. S.; Seeger, R.; Pople, J. A. *J. Chem. Phys.* **1980**, *72*, 650.
(52) Wachters, A. J. *J. Chem. Phys.* **1970**, *52*, 1033.
(53) Hay, P. J. *J. Chem. Phys.* **1977**, *66*, 4377.
(54) Raghavachari, K.; Trucks, G. W. *J. Chem. Phys.* **1989**, *91*, 1062.

convergence criterion was set to 0.000667 au using IOP 1/7. Stationary points were analyzed by performing analytical frequency calculations. An inevitable consequence of the fixing approach described above is that some of the structures with H_2 bound have imaginary frequencies. These are generally very few (no more than two) and small in magnitude (typically <30i cm^{-1}). All imaginary frequencies are isolated in the part of the molecules that are fixed prior to interaction with H_2.

Partial atomic charges were quantified using the Mulliken, Voronoi, and Hirshfeld scales. These were calculated using the Amsterdam Density Functional (ADF) program,[57−59] with PBE and TZ2P basis sets[60−64] on all the atoms, at the Gaussian-optimized geometries, and the Mulliken values were also calculated using Gaussian.

The enthalpy, per H_2 unit, of the reaction between a binding site representation (BSR) and n H_2 molecules was calculated as the difference in energy between the reactants and the products divided by the number of H_2 molecules, that is, for

$$\mathrm{BSR} + n\mathrm{H_2} \rightarrow \mathrm{BSR(H_2)}_n$$

$$\Delta H_{\mathrm{H_2}} = \frac{E_{\mathrm{BSR(H_2)}_n} - E_{\mathrm{BSR}} - nE_{\mathrm{H_2}}}{n}$$

E for all species was taken as the SCF energies from the Gaussian optimizations, corrected with zero point energies and thermal corrections to 298 K.

The Ti−H_2 interaction energies were calculated using the Ziegler−Rauk[65] energy decomposition scheme implemented in the ADF code, with TZ2P basis sets[60−64] on all the atoms and the Gaussian-optimized geometries. Default SCF convergence criteria were used, and the parameter controlling the integration grid was set to 6.0. The molecules were split into two fragments: the H_2 units and the rest of the molecule. The Ti−H_2 interaction energy per H_2 molecule was found by dividing by the number of H_2 molecules bound. The Ti−H_2 interaction energies were corrected for BSSE (∼1 kJ mol^{-1} per H_2 molecule bound) using the counterpoise method.

The Ziegler−Rauk scheme requires the use of spin-restricted fragments. This is appropriate for the titanium systems, for which the metal fragment has one unpaired electron, but not so for the vanadium and chromium species. For the latter, the average energy of interaction between the metal and the H_2 units was calculated in ADF as follows. Using the same functional, basis set, and integration grid as for the titanium Ziegler−Rauk calculations, and geometries of the $BSR(H_2)_n$ species from the Gaussian optimizations, a spin-unrestricted single point calculation was performed. Two further single point calculations were then performed breaking the molecule into two fragments: the metal-containing fragment (spin-unrestricted) and the $(H_2)_n$ fragment (spin restricted). The average energy of interaction between the metal and the H_2 units was calculated as

$$E^{\mathrm{int}}_{\mathrm{H_2}} = \frac{E_{\mathrm{BSR(H_2)}_n} - E_{\mathrm{BSR}} - E_{\mathrm{(H_2)}_n}}{n}$$

E for all species was taken as the SCF energies. To facilitate comparison, any Ti−H_2 interaction energies quoted in the context of comparison with analogous vanadium and chromium data were recalculated using the spin-unrestricted method.

3. Results and Discussion

3.1. The Titanium−Benzyl System. Table 1 summarizes the molecules identified in this study and gives the number of H_2 units, the H−H bond lengths, and stretching frequencies. We begin by discussing the result for Ti with benzyl ancillary ligands, to benchmark the computational method against experiment. The maximum number of H_2 molecules that can be bound to binding site representation (BSR) (a) is three (Figure 2D) and to BSR (b) is four (Figure 2I). This agrees well with the maximum found to bind experimentally of 4.85 H_2 per Ti.[35]

The average Ti−H_2 reaction enthalpies $\Delta H_{\mathrm{H_2}}$ and interaction energies $E^{\mathrm{int}}_{\mathrm{H_2}}$ are compared to the experimental hydrogen adsorption enthalpies in Figure 3, from which it may be seen that the calculated reaction enthalpies do not agree very well with experiment. This can be traced to the distortions that occur when a BSR accommodates incoming H_2 molecules. These distortions carry energy penalties that are larger than the energy recovered through Ti−H_2 bond formation (see Supporting Information Tables 1 and 2), and the calculated reaction enthalpies are positive. It is likely that, in the extended solid of the experimental system, the binding sites will be less free to distort on introduction of H_2, and hence the enthalpies are dominated more by Ti−H_2 bond formation. This is supported by our calculated Ti−H_2 interaction energies, which agree rather better with experiment, deviating by at most ca. 10 kJ mol^{-1}. It is also notable that the Ti−H_2 interaction energies generally increase as the number of H_2 units increases, as observed experimentally and in the previous computational studies of Zhao et al.[19] and Lee et al.[28] on the binding of H_2 to Sc-decorated fullerenes and Ti−C_2H_2, respectively. We will use the M−H_2 interaction energies, rather than H_2 reaction enthalpies, throughout this Article.

On binding to titanium, the H−H bond lengthens from its calculated free value of 0.752 Å to between 0.77 and 0.79 Å, and the H−H stretching frequency reduces from its free value of 4315 cm^{-1} to between 3635 and 3966 cm^{-1} (Table 1). To establish if these effects arise as the result of Kubas interactions, we have analyzed the molecular orbital (MO) structure of the target compounds. Figure 4 shows three-dimensional images of MOs of the titanium-benzyl BSR (b) with four H_2 units attached. MOs displaying σ-donation from the H_2 σ-bonding orbitals to d-based orbitals on the metal (Figure 4A−C) and π-back-donation from d-based orbitals to the σ^* antibonding orbital of the H_2 molecules (Figure 4D and E) can be identified (several of these MOs also contain contributions from the ancillary benzyl ligands). We therefore conclude that the lengthening of the H−H bonds and reduction in stretching frequencies are the result of Kubas interactions, in agreement with the hydrogen adsorption enthalpies of the experimentally characterized material lying between those of typical physisorption and dissociative chemisorption interactions. This is important because no compound has yet been isolated with more than two H_2 molecules bound in a Kubas fashion, and hence the conclusion that our experimental system can bind up to four H_2 units via a Kubas mechanism is significant.

(55) Clark, T.; Chandrasekhar, J.; Spitznagel, G. W.; Schleyer, P. V. *J. Comput. Chem.* **1983**, *4*, 294.
(56) Frisch, M. J.; Pople, J. A.; Binkley, J. S. *J. Chem. Phys.* **1984**, *80*, 3265.
(57) Velde, G. T.; Bickelhaupt, F. M.; Baerends, E. J.; Guerra, C. F.; Van Gisbergen, S. J. A.; Snijders, J. G.; Ziegler, T.; Chemistry with, A. D. F. *J. Comput. Chem.* **2001**, *22*, 931.
(58) Guerra, C. F.; Snijders, J. G.; te Velde, G.; Baerends, E. J. *Theor. Chem. Acc.* **1998**, *99*, 391.
(59) *ADF2009.01*; SCM: Amsterdam, 2009.
(60) Raffenetti, R. C. *J. Chem. Phys.* **1973**, *59*, 5936.
(61) Chong, D. P. *Can. J. Chem.* **1995**, *73*, 79.
(62) Zeiss, G. D.; Scott, W. R.; Suzuki, N.; Chong, D. P.; Langhoff, S. R. *Mol. Phys.* **1979**, *37*, 1543.
(63) Van Lenthe, E.; Baerends, E. J. *J. Comput. Chem.* **2003**, *24*, 1142.
(64) Chong, D. P.; Van Lenthe, E.; Van Gisbergen, S.; Baerends, E. J. *J. Comput. Chem.* **2004**, *25*, 1030.
(65) Ziegler, T.; Rauk, A. *Theor. Chim. Acta* **1977**, *46*, 1.

Table 1. Number of Bound H_2 Units, H−H Bond Lengths (Å), and Stretching Frequencies (cm^{-1}) for All of the Geometries Located[a]

		H−H bond lengths						H−H stretching frequencies					
		BSR (a)			BSR (b)			BSR (a)			BSR (b)		
ancillary ligand	no. H_2 bound	Ti	V	Cr	Ti	V	Cr	Ti	V	Cr	Ti	V	Cr
benzyl	1	0.787	0.790	0.770	0.792	0.785	0.773	3721	3685	4036	3635	3766	3967
	2	0.773	0.780	/	0.786	0.781	/	3972	3932	/	3888	3847	/
		0.772	0.776		0.777	0.781		3959	3852		3730	3832	
	3	0.784	/	/	0.788	0.786	/	4048	/	/	3827	3843	/
		0.776			0.786	0.786		3883			3752	3770	
		0.768			0.780	0.781		3762			3669	3754	
	4	/	/	/	0.776	/	/	/	/	/	3947	/	/
					0.776						3912		
					0.775						3902		
					0.773						3893		
hydride	1	0.827	0.812	0.782	0.815	0.834	0.764	3131	3364	3834	3313	3103	4120
	2	0.788	0.793	0.797	0.813	0.827	/	3841	3731	3625	3428	3367	/
		0.779	0.788	0.796	0.807	0.814		3687	3645	3611	3340	3187	
	3	/	0.792	0.818	0.813	/	/	/	3923	3856	3707	/	/
			0.788	0.801	0.800				3722	3555	3524		
			0.776	0.782	0.787				3661	3312	3351		
	4	/	/	/	0.803	/	/	/	/	/	3893	/	/
					0.802						3751		
					0.785						3514		
					0.777						3475		
methyl	1	0.807	0.796	0.769	0.810	0.796	0.781	3398	3599	4049	3353	3590	3845
	2	0.783	0.784	0.774	0.781	0.783	0.785	3896	3965	4086	3843	3903	3876
		0.776	0.774	0.769	0.780	0.777	0.780	3769	3788	3962	3790	3803	3805
	3	/	/	0.790	0.790	0.801	0.806	/	/	3908	3962	3849	3726
				0.784	0.778	0.783	0.797			3811	3869	3806	3606
				0.778	0.773	0.780	0.790			3721	3641	3547	3480
	4	/	/	/	0.780	/	/	/	/	/	3924	/	/
					0.779						3871		
					0.777						3853		
					0.774						3836		
allyl	1	0.783	*	*	0.779	*	*	3793	*	*	3843	*	*
	2	0.782	*	*	0.794	*	*	3862	*	*	3906	*	*
		0.777			0.776			3782			3621		
	3	0.788	*	*	0.798	*	*	4049	*	*	3945	*	*
		0.776			0.781			3884			3789		
		0.769			0.774			3686			3553		
	4	/	*	*	0.782	*	*	/	*	*	3955	*	*
					0.778						3943		
					0.774						3868		
					0.772						3803		

[a] BSR = binding site representation (see Figure 1 for definition of BSR (a) and BSR (b)). / = geometry did not optimize. * = optimization not attempted.

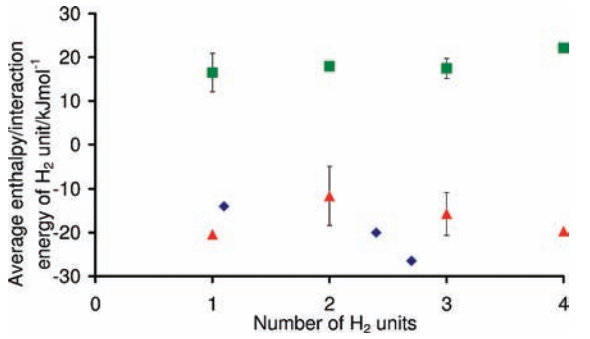

Figure 3. Comparison between the experimental hydrogen adsorption enthalpies[33] (blue) and the computational Ti−H_2 interaction energies (red) and hydrogen reaction enthalpies (green). The experimental enthalpies are an average over all sites in the solid. The computational interaction energies and reaction enthalpies are each an average over the two binding site representations, and the error bars show the range of these values.

Figure 5 shows how the partial charge on the metal in titanium−benzyl BSR (a) decreases as the number of bound H_2 molecules increases. Although the absolute values of the partial charges vary considerably as a function of analysis method and code/basis set, all approaches agree that as more H_2 are bound the Ti gains electron density, as was observed by Zhang et al. in their study of Ti-substitued boranes (the partial charge on the Ti in B_5H_5Ti reduces from +1.24 with no bound H_2 to −0.82 with five bound H_2).[30] The reduction in partial charge suggests that the interaction is overall a donation from the H_2 molecule(s) to the Ti, consistent with the increase in H−H bond length and reduction in stretching frequency, as electron density is removed from the H_2 σ-bonding orbital.

3.2. Altering the Ancillary Ligand. The maximum number of H_2 molecules that can be bound to the Ti atom when the benzyl ancillary ligands are replaced by hydride, methyl, or allyl is two, two, and three, respectively, for BSR (a), and four to all BSRs (b) (Table 1 and Figure 6). The Ti−H_2 interaction energies when one H_2 molecule is bound decrease for both BSRs in the order hydride > methyl > benzyl > allyl (Table 2). For more than one H_2, it is generally the case that the Ti−H_2 interaction energies are by far the largest for the hydride compounds, with some variations in the ordering of the other ancillary ligands. Hydride < methyl < benzyl < allyl is the generally accepted

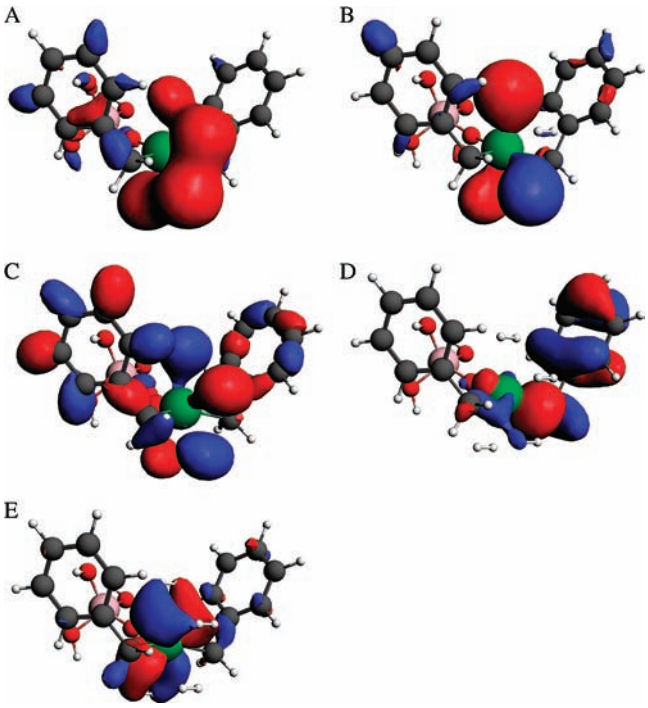

Figure 4. Three-dimensional representations of selected molecular orbitals from titanium−benzyl binding site representation (b) with four H_2 molecules bound: (A) HOMO−39, (B) HOMO−33, (C) HOMO−31, (D) HOMO−1, and (E) HOMO.

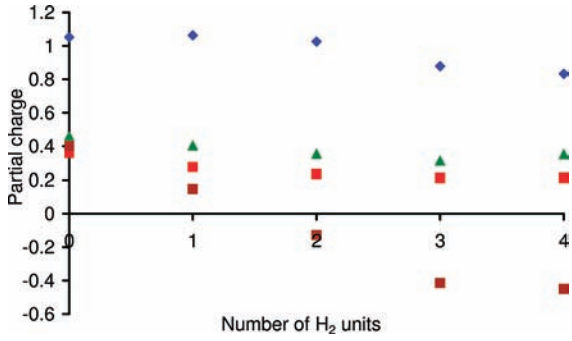

Figure 5. The partial charge on the metal in titanium−benzyl binding site representation (a) as a function of the number of H_2 molecules bound. Blue, ADF Mulliken; red, ADF Voronoi; green, ADF Hirshfeld; and brown, Gaussian Mulliken.

order of increasing ability to π-accept electron density.[66] The more that the ancillary ligand can π-accept electron density from the metal, the less electron density that is available for π-back-donation to the H_2 molecule and the weaker is the Ti−H_2 interaction. This conclusion is reminiscent of the study of Lee et al., in which it was found that the initial Ti−H_2 binding energy decreased when the ancillary ligands were altered from thiol/hydroxide to acetylene.[28]

The spatial overlap between the frontier molecular orbitals of the BSR and those of the H_2 molecule should also affect the strength of the Ti−H_2 interaction. If the Ti atom is sterically hindered, the H_2 may not be able to approach it to achieve optimum overlap, and the Ti−H_2 interaction may be weaker. The ancillary ligands should increase the steric hindrance of the Ti in the order hydride < methyl < allyl < benzyl. BSRs with hydride ancillary ligands presumably achieve significantly higher Ti−H_2 interaction energies as not only does the hydride ancillary ligand not possess any orbitals that could take part in π-acceptance from the metal, but also it poses very little steric hindrance.

(66) Huheey, J. E.; Keiter, E. A.; Keiter, R. L. *Inorganic Chemistry: Principles of Structure and Reactivity*, 4th ed.; Harper Collins College Publishers: New York, 1993.

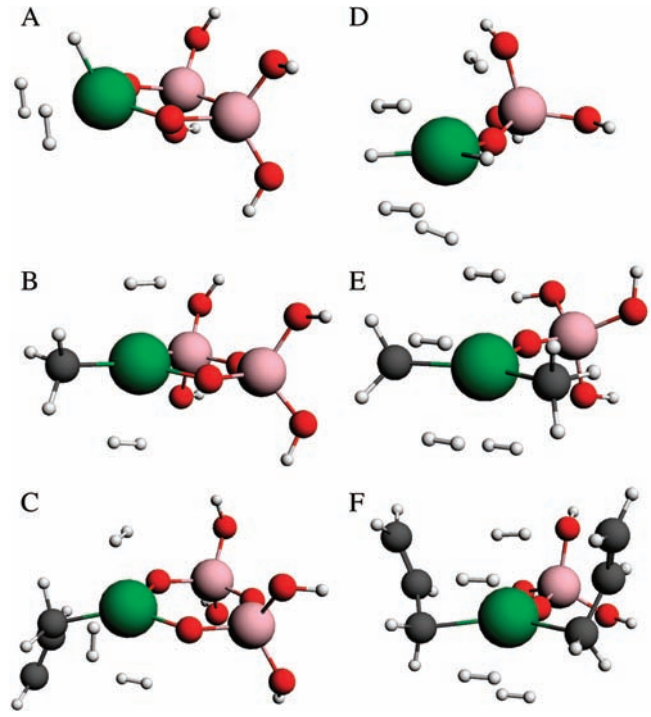

Figure 6. Ball-and-stick representations of the optimized geometries of the molecules with the maximum number of bound H_2. Binding site representation (a) with (A) hydride ancillary ligand and two H_2 molecules bound, (B) methyl ancillary ligand and two H_2 molecules bound, and (C) allyl ancillary ligand and three H_2 molecules bound. Binding site representation (b) with four H_2 molecules bound with (D) hydride, (E) methyl, and (F) allyl ancillary ligands.

Table 2. Average Ti−H_2 Interaction Energy (kJ/mol) of Binding Site Representations (a) and (b) as the Ancillary Ligand Is Varied

		number of H_2 units bound			
BSR	ancillary ligand	1	2	3	4
(a)	allyl	−17.56	−23.97	−12.87	
	benzyl	−21.63	−6.13	−11.91	
	methyl	−30.61	−8.55		
	hydride	−53.86	−33.82		
(b)	allyl	−16.45	−22.03	−16.13	−20.72
	benzyl	−21.63	−19.69	−21.80	−20.76
	methyl	−31.15	−20.00	−17.47	−23.05
	hydride	−57.15	−54.75	−51.00	−38.25

Table 3. Average V−H_2 Interaction Energy (kJ/mol) of Binding Site Representation (a) as the Ancillary Ligand Is Varied

	number of H_2 units bound		
ancillary ligand	1	2	3
benzyl	−19.08	−15.15	
methyl	−29.95	−15.59	
hydride	−43.28	−24.16	−25.30

3.3. Altering the Metal. We now examine the effect of altering the metal from Ti to V or Cr on the M−H_2 interaction, for all ancillary ligands bar allyl. Table 3 shows the variation in the V−H_2 interaction energy as the benzyl ancillary ligand is altered to methyl or hydride. The V−H_2 interaction energies

Table 4. Average M−H_2 Interaction Energy (kJ/mol) as a Function of the Number of Bound H_2 Molecules for Binding Site Representation (a) with Benzyl, Methyl, or Hydride Ancillary Ligands and Different Metal Atoms

		number of H_2 units bound		
ancillary ligand	metal	1	2	3
benzyl	Ti	−15.95	−0.07	−7.49
	V	−19.08	−15.15	
	Cr	−15.24		
methyl	Ti	−23.67	−5.03	
	V	−29.95	−15.59	
	Cr	−12.94	−16.27	−20.11
hydride	Ti	−47.54	−30.42	
	V	−43.28	−24.16	−25.3
	Cr	−23.27	−10.45	−33.14

decrease in the order hydride > methyl > benzyl for both one and two bound H_2 molecules. This is the same order as for Ti; that is, the trends in the H_2 molecule bonding observed upon changing the ancillary ligand appear to be independent of the metal atom used. Similar data for Cr are not shown as it proved impossible to bind more than one H_2 molecule with a benzyl ancillary ligand (Table 1).

Table 4 shows how the M−H_2 interaction energy of BSR (a) with a hydride, methyl, or benzyl ancillary ligand, respectively, varies with metal atom and with the number of bound H_2 molecules. It is clear that, for a given ancillary ligand, the variation in the M−H_2 interaction energy as more H_2 are bound is not the same for all metals, reminiscent of the work of Zhou et al., who found little pattern in the consecutive M−$(H_2)_n$ binding energies ($n = 2-4$) in H_2 binding to M−C_5H_5 as M was varied from Sc to Mn.[19]

The energies of the metal d-based frontier orbitals that form the HOMOs and LUMOs that bind the incoming H_2 are affected by several factors, including (i) the number of filled d orbitals, (ii) the lowering in d orbital energies from Ti to Cr across the periodic table, and (iii) the minimum energy ligand coordination geometries about the metal centers, which cause different d orbital splitting patterns. First-order perturbation theory tells us that two factors contribute to orbital mixing: orbital overlap and the energy difference between the orbitals. Thus, for better mixing between the fragment orbitals, and a strong Ti−H_2 interaction, the BSR requires a high-energy HOMO to interact with the H_2 molecule's high-energy LUMO (0.72 eV) and a low-energy LUMO to interact with the H_2 molecule's low-energy HOMO (−10.36 eV). As we shall see, for a given ancillary ligand, the M−H_2 interaction energies track the HOMO and LUMO energies, at least in a qualitative sense; that is, the BSRs with highest energy HOMOs and lowest energy LUMOs bond to the next H_2 molecule to form the strongest M−H_2 interaction. We present the orbital-based rationalization of M−H_2 interaction energies for BSRs with hydride and benzyl ancillary ligands. Analogous changes in the M−H_2 interaction energies for all of the considered ancillary ligand/metal combinations may in general be explained using arguments similar to those set out below (see Supporting Information Figures 2−4).

Figures 7−9 present valence molecular orbital energy level diagrams for Ti, V, and Cr, respectively, for BSR (a) with a hydride ancillary ligand. Indicated on these diagrams are the orbitals responsible for binding a given incoming H_2 (to produce the structure immediately to the right). These orbitals were located as follows. The M−H_2 σ-bonding and π-bonding orbitals in the molecule with the H_2 bound were identified, and the metal d character of these orbitals was established. Those frontier MOs in the molecule without the H_2 bound, which have the appropriate d character, are then taken as the interacting frontier orbitals. If there is more than one orbital with the correct d character, then an unweighted average of the orbitals' energies is taken as the energy of the interacting HOMO or LUMO.

The MO diagrams can help to explain the trend in the M−H_2 interaction energies as a function of the number of H_2 molecules bound. For example, the Ti−H_2 interaction energy with a hydride ancillary ligand decreases on going from one to two bound H_2 molecules (Table 4). In the corresponding molecular orbital diagram (Figure 7) with no bound H_2, the HOMO (−3.67 eV) and LUMO (−3.15 eV), which bind to the incoming H_2 molecule, are more favorable in energy (higher and lower, respectively) for binding than the HOMO (−3.78 eV) and LUMO (−2.13 eV) when one H_2 molecule is bound. A third H_2 molecule does not bind. This may well be because the $3d_{z2}$-based LUMO of BSR$(H_2)_2$, which would interact with the incoming H_2 molecule, is high in energy (−1.27 eV).

The V−H_2 and Cr−H_2 interaction energies with a hydride ancillary ligand increase on moving from two bound H_2 molecules to three (Table 4). This may be explained by the corresponding molecular orbital diagrams (Figures 8 and 9). For V and Cr, the interacting HOMO energy rises by 0.35 and 1.07 eV, respectively, and the average energy of all the interacting LUMOs falls by 0.15 and 0.2 eV, respectively, on going from one to two bound H_2. Thus, the orbitals become more favorable in energy to interact with the HOMO and LUMO of the incoming third H_2 molecule, and the M−H_2 interaction energies increase (more so for Cr than V as the HOMO energy change is larger in the d^3 system).

For the experimental (benzyl) system, the Ti−H_2 interaction energies are smaller than for the compounds with hydride ancillary ligands, as are the changes in the interaction energies as a function of the number of bound H_2. We might, therefore, expect the changes in the interacting orbital energies to be smaller for the benzyl systems than is the case for the hydride molecules. Figures 10 and 11 present molecular orbital energy level diagrams of the two BSRs of the experimental system. Comparison of these with Figure 7, the analogous diagram for titanium−hydride BSR (a), reveals a further factor, which should lead to the orbital energy changes being smaller in the benzyl case. The interacting LUMOs (those orbitals responsible for the σ accepting component of the Kubas interaction) are significantly less metal-based in the benzyl systems than for the hydride. Thus, the interacting LUMO in BSR (a) for the hydride molecules is 74%, 41%, and 45% Ti d-based, respectively, with zero, one, and two bound H_2. By contrast, the analogous orbital for the benzyl molecules contains only 33%, 25%, and 21% Ti d character. This reduction in metal d character from hydride to benzyl should reduce the changes in orbital energy as H_2 are bound, as more of the orbital is localized away from the metal/H_2 interaction region.

Comparison of Figures 10, 11, and 3 indicates that in some cases the changes in interacting MO energies correlate with the interaction energies, but not in others. For example, on going from one to two bound H_2 for BSR (b), the HOMO energy rises by 0.05 eV, and the average interacting LUMO energy lowers by 0.08 eV. This closer energy match with the incoming H_2 levels makes it more favorable to bind the next H_2 molecule, and this agrees with the increase in the Ti−H_2 interaction energy. However, for BSR (a), both the HOMO and the LUMO energies rise by 0.09 eV. Thus, in this case, the interacting energy levels show no favorability in energy for binding the next H_2, which

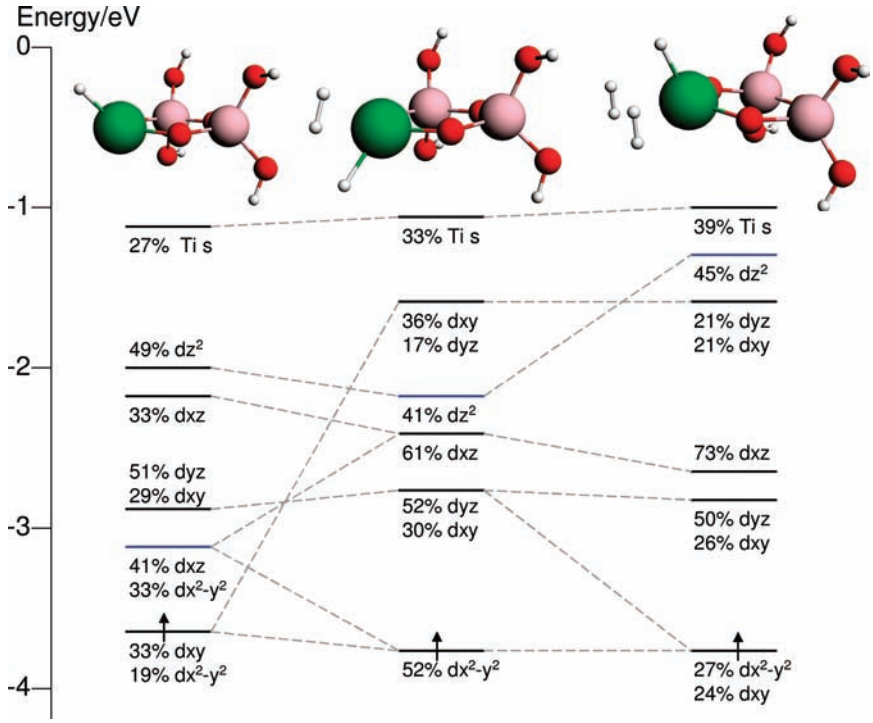

Figure 7. Molecular orbital energy level diagram of titanium−hydride binding site representation (a) with zero, one, and two bound H_2 molecules. The d-based electron in the HOMO of each molecule is indicated by an arrow. The interacting LUMOs are indicated by the blue lines.

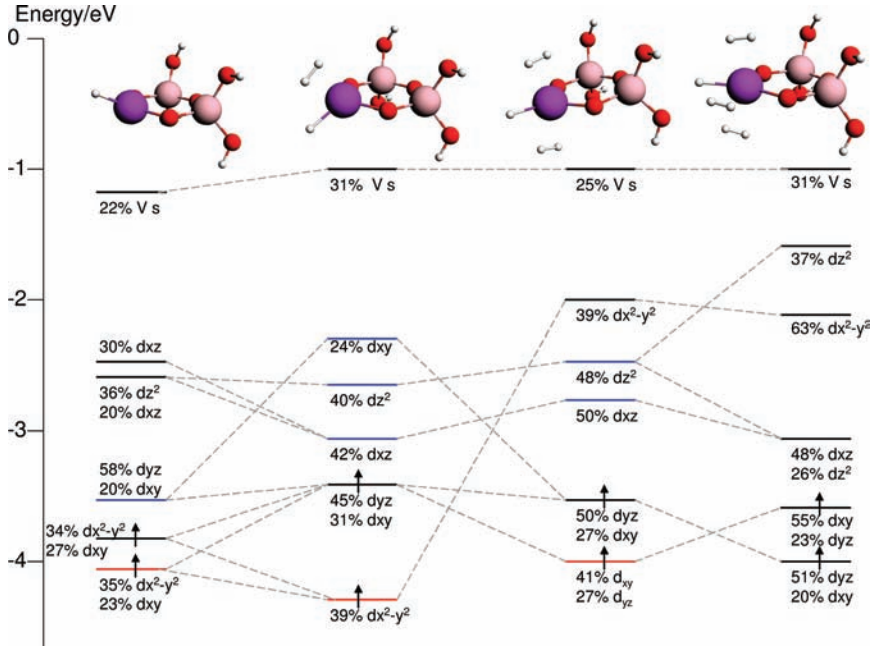

Figure 8. Molecular orbital energy level diagram of vanadium−hydride binding site representation (a) with zero, one, two, and three bound H_2 molecules. The d-based electrons in the HOMOs of each molecule are indicated by arrows. The interacting HOMOs and LUMOs are indicated by the red and blue lines, respectively.

does not agree with the increase in the Ti−H_2 interaction energy. However, the overall change in the energy of the interacting levels is very small, and we must be cautious about rationalizing the M−H_2 interaction energy change in these circumstances.

Table 5 presents the energies of the interacting HOMOs and LUMOs of BSR (a) with hydride ancillary ligands for Ti, V, and Cr. When one H_2 molecule is bound, the order of the M−H_2 interaction energies is Ti > V ≫ Cr (Table 4). Consideration of the HOMO and LUMO energies of the BSRs without bound H_2 reveals that Cr has by far the largest HOMO−LUMO gap (1.63 eV), with the lowest HOMO (−4.55 eV) and the highest LUMO (−2.92 eV), in agreement with Cr-BSR (a) having the smallest M−H_2 interaction energy for one H_2. The V−H_2 and Ti−H_2 interaction energies for one H_2 are very similar to one another, and much larger than for Cr. Ti-BSR (a) has the higher HOMO (−3.67 eV) and higher LUMO (−3.15 eV), while V-BSR (a) has the lower HOMO (−4.09 eV) and lower LUMO (−3.54 eV), resulting in significantly smaller HOMO−LUMO

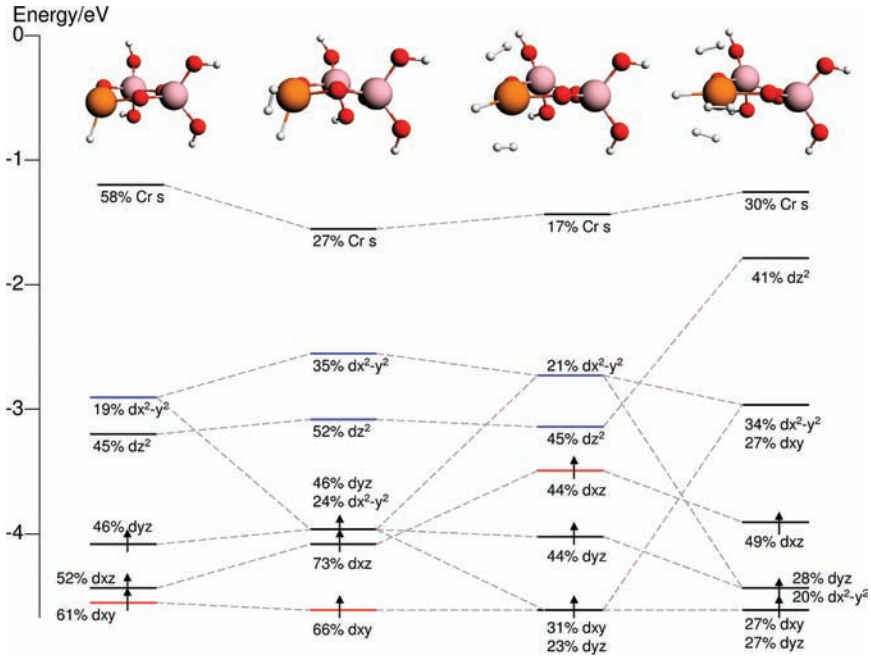

Figure 9. Molecular orbital energy level diagram of chromium−hydride binding site representation (a) with zero, one, two, and three bound H_2 molecules. The d-based electrons in the HOMOs of each molecule are indicated by arrows. The interacting HOMOs and LUMOs are indicated by the red and blue lines, respectively.

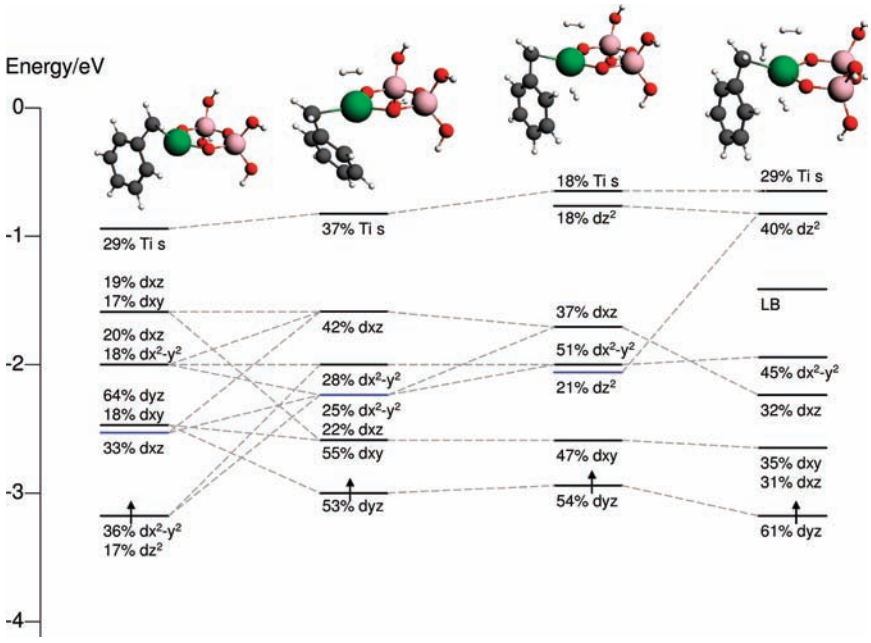

Figure 10. Molecular orbital energy level diagram of titanium−benzyl binding site representation (a) with zero, one, two, and three bound H_2 molecules. The d-based electron in the HOMO of each molecule is indicated by an arrow. The interacting LUMOs are indicated by the blue lines. LB = ligand-based orbital.

gaps than for the Cr system (0.52 and 0.55 eV, respectively, for Ti and V). Although the energies of the frontier orbitals in V-BSR (a) are overall very slightly less favorable for interaction with the incoming H_2 than the Ti complex, in agreement with the slightly larger Ti−H_2 interaction energy, as noted above, caution must be exercised over quantitative usage of such small orbital energy differences.

When two H_2 molecules are bound to hydride BSR (a), the order of the average M−H_2 interaction energies is once again Ti > V ≫ Cr (Table 4), with all being significantly reduced from the value for one H_2. Table 5 shows that the energies of all the HOMOs are stabilized on going from zero to one bound H_2, and the LUMOs are all destabilized, in agreement with the smaller average M−H_2 interaction energies in the complexes with two H_2. As for the case of the molecules with no bound H_2, the HOMO−LUMO gap for one bound H_2 is largest for Cr, in agreement with this metal having the smallest average interaction energy when two H_2 are bound.

Table 4 shows that the average Cr−H_2 interaction energy increases significantly on going from two to three bound H_2, very much in agreement with the HOMO−LUMO gap reducing from ca. 1.80 eV for the Cr molecule with one bound H_2 to

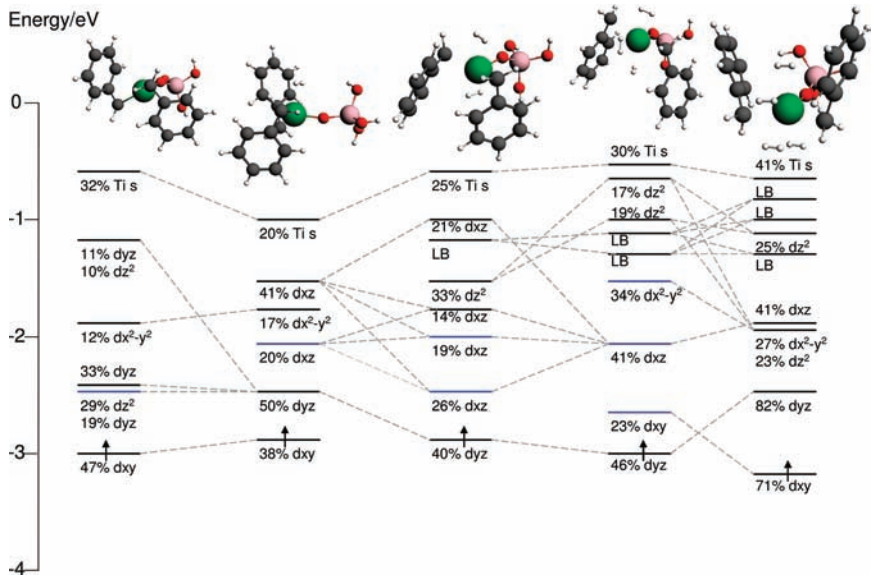

Figure 11. Molecular orbital energy level diagram of titanium−benzyl binding site representation (b) with zero, one, two, three, and four bound H_2 molecules. The d-based electron in the HOMO of each molecule is indicated by an arrow. The interacting LUMOs are indicated by the blue lines. LB = ligand-based orbital.

Table 5. Energies (eV) of the HOMOs and LUMOs of Binding Site Representation (a) with a Hydride Ancillary Ligand and Different Metals, Which Subsequently Bind to the Next H_2 Molecule

	number of H_2 units bound					
	0		1		2	
metal	HOMO	LUMO	HOMO	LUMO	HOMO	LUMO
Ti	−3.67	−3.15	−3.78	−2.13	−3.74	−1.27
V	−4.09	−3.54	−4.33	−2.7 ± 0.4	−3.98	−2.7 ± 0.1
Cr	−4.55	−2.92	−4.64	−2.8 ± 0.3	−3.58	−3.0 ± 0.2

only 0.58 eV when two H_2 are bound (primarily due to the favorable destabilization of the interacting HOMO). The V HOMO−LUMO gap reduces from ca. 1.6 to 1.28 eV on going from two to three bound H_2, in agreement with the V−H_2 interaction energy reducing slightly and with the order of the interaction energies when three H_2 molecules are bound of Cr−H_2 > V−H_2.

4. Conclusions

In this Article, we have presented a quantum chemical computational model of the titanium−H_2 binding sites of a mesoporous silica, which has successfully reproduced the experimentally determined maximum number of bound H_2 molecules per Ti. We find the average Ti−H_2 interaction energies in these molecular models of the experimental systems (i.e., incorporating benzyl ancillary ligands) to increase as the number of bound H_2 units increases from two to four, in agreement with the experimental observation that the H_2 adsorption enthalpy increases as the number of adsorbed H_2 molecules increases.[32,33]

Analysis of the valence molecular orbital structures shows the Ti−H_2 interactions to be of a synergic Kubas type. It is found that when the ancillary ligand is altered from benzyl to allyl, methyl, or hydride, the average M−H_2 interaction energy decreases as the ancillary ligand becomes a better π-acceptor and the more sterically hindered it causes the metal center to be. Extension of the calculations to V and Cr showed that the variations in the M−H_2 interaction energy as a function of metal are not independent of the ancillary ligand, and detailed analysis of the valence molecular orbital structures has provided a rationalization for these variations.

In summary, this Article confirms the role of Kubas binding in silica-supported transition metal fragments and establishes a theoretical framework for the rising enthalpy trends observed with surface coverage. While more spectroscopic and physical studies are needed to determine the exact values for binding enthalpies in these systems, this Article supports a series of experimental results, the explanation of which has until now remained elusive. We anticipate that the computational model presented here may be applied to other systems both to explain the trends in the hydrogen adsorption enthalpies and to predict the effect of changes (e.g., of ligand and/or metal) on hydrogen adsorption properties. We are applying our model to the hydrazine-based systems currently under study.[34]

Acknowledgment. We are grateful to the UCL Graduate School for a scholarship to C.V.J.S., and for computing resources via UCL's Research Computing "Legion" cluster and associated services.

Supporting Information Available: Several figures, referred to in the main text, together with atomic coordinates, vibrational frequencies, and total SCF energies of all structures calculated. Full version of ref 49. This material is available free of charge via the Internet at http://pubs.acs.org.

JA107539J